

Chapter 15

Dimensional Engineering of 2D/3D Perovskite Halides for Efficient and Stable Solar Cells



Arif D. Sheikh and Kiran Kumar K. Sharma

Abbreviations

3D	Three-dimensional
2D	Two-dimensional
1D	One-dimensional
0D	Zero-dimensional
PCE	Power conversion efficiency
PSCs	Perovskite solar cells
MA	Methyl ammonium (CH_3NH_3^+) ion
FA	Formamidinium ($\text{HC}(\text{NH}_2)_2^+$) ion
ETL	Electron transporting layer
HTL	Hole transporting layer
DSSCs	Dye-sensitized solar cells
CZTS	Copper zinc tin sulfide ($\text{Cu}_2\text{ZnSnS}_4$)
spiro-OMeTAD	2,2',7,7'-Tetrakis(N,N-pdimethoxyphenylamino)-9,9'-spirobifluorene
PEDOT	PSS-poly(3,4-ethylenedioxythiophene) polystyrene sulphonate
PTAA	Poly[bis(4-phenyl)(2,4,6-trimethylphenyl)amine]
P3HT	Poly(3-hexylthiophene-2,5-diyl)
ABHB	4-(Aminomethyl)benzoic acid hydrogen bromide
GBL	Gamma butyrolactone

A. D. Sheikh (✉)

Center for Nanoscience and Nanotechnology, Amity University Maharashtra, Bhatan, Panvel, Mumbai 410206, Maharashtra, India
e-mail: adsheikh@mum.amity.edu

K. K. K. Sharma (✉)

School of Nanoscience and Biotechnology, Shivaji University, Kolhapur 416004, Maharashtra, India
e-mail: kks.snst@unishivaji.ac.in

DMSO	Dimethyl Sulphoxide
MQWs	Multi-quantum wells
QWs	Quantum wells
LP-VASP	Low-Pressure Vapor-assisted Solution Process
FF	Fill factor
WBH	Wide-bandgap halide
FESEM	Field emission scanning electron microscopy
RH	Relative humidity
V_{oc}	Open circuit voltage
GIXRD	Grazing Incidence X-ray diffraction
FTO	Fluorine-doped tin oxide

15.1 Introduction

In the era of the Internet of Things, artificial intelligence, machine learning, and the rapid development of the world, the use of electronic devices relentlessly demands alternative, renewable, and carbon-neutral energy sources. In recent years, the world storage of coal, crude oil, natural gas, and other non-renewable energy sources are impacting climate change and the environment's global warming issue. With time, the problem of energy shortage is becoming more severe for the development of the global economy. Against this background, most countries continuously focus on harvesting energy using alternative sources like wind, geothermal, photovoltaics, hydrogen generation, solar thermal power plants, etc. All these types of renewable energy sources could effectively promote economic growth, enhance energy security, increase energy access, and reduce carbon footprint (Satapathi 2022). Among different renewable energy sources, solar energy is the largest available source that has the potential for scaling up to meet future energy demands. The solar energy supply to the earth's surface is gigantic: 3×10^{24} J per year (Grätzel 2001). In principle, the complete conversion of solar energy that strikes the surface of the globe in 1 h into electricity can fulfill the current global energy consumption of an entire year required for humanity. It is predicted that harvesting less than 0.02% of the solar energy that falls on the earth's surface would satisfy the present needs (Hammarström and Hammes-Schiffer 2009). Solar cells can straightforwardly transform light into electricity through the photovoltaic effect, and currently, silicon solar cell is the most sophisticated commercialized technology. Nevertheless, because of the complexity of the fabrication technique and the excessive cost of silicon materials, it remained a bottleneck for the absorption of the technology to ground level. Despite this present Si-based photovoltaic technology, finding alternative cost-effective materials and methods to fabricate economical solar cells is necessary. The dye-sensitized solar cells (DSSCs), CZTS-based solar cells, organic solar cells, and quantum dot solar cells are some of the alternative types of solar cells, which are focused on for the last couple of decades. However, even after the success so far achieved with solar

cells, their low photo conversion efficiency (PCE) and lack of low-cost solution processing techniques still remain a bottleneck. In the last decade, hybrid perovskite halide-based solar cells have developed as an emerging era of promising low-cost solution-processed photovoltaic technologies.

The most studied inorganic–organic hybrid perovskites like MAPbI₃, FAPbI₃, and CsPbI₃ and their compositions have attracted considerable attention due to their superior electronic and optoelectronic properties resulting in spectacular successes in solar cell applications. Various strategies are used to improve the PCE of PSCs from 3.8% to 25% through the optimization and processing of various device architectures (Cell-Efficiency n.d.). The PSCs are the first category based on ultra-low-cost fabrication via low-temperature solution processing techniques with high efficiency close to commercial Si solar cells of 25% and have a high potential for integrated photovoltaics (Liang et al. 2021; Gangadharan and Ma 2019). Unfortunately, these conventional hybrid perovskite materials are sensitive to humidity, thermal cycling, ultraviolet radiations, and ion migration due to the volatile nature of the organic group (Schileo and Grancini 2020; Sheikh et al. 2015, 2017). This instability of 3D perovskite halides under extreme ambient conditions like moisture, heat, oxygen, and a significant roadblock remains to be the ultraviolet light for the commercialization of perovskite-based photovoltaic technology. Therefore, even after surpassing the photoconversion efficiency of PSCs, issues regarding ambient stability need to be resolved. Over the past decade, the PCE of PSCs performance and stability was improved by numerous strategies employed by the researchers including device encapsulation techniques (Ma et al. 2022), compositional and solvent engineering (Jeon et al. 2015, 2014a), dopant/additive incorporation (Ugur et al. 2017), selection and modification of charge transporting materials/layers (Haque et al. 2017), implementation of novel metal electrodes (Lee et al. 2019), and dimensional engineering of perovskite film (Krishna et al. 2019; Zhang et al. 2018). Among these, the research on engineering of low-dimensional perovskite materials has drawn tremendous interest because of the remarkable progress made in both device efficiency and the stability of PSCs.

This chapter is focused on the fundamental understanding of dimensional engineering of perovskite halides and explored recent advances reported in the literature. In the dimensional engineering strategy, one can modify the size and shape of the material at the nanoscale by tuning the processing parameters and precursors. Further, introduced the basics of 3D perovskite and 2D perovskite materials and elaborated on their use in PSCs. Recent research demonstrated that 2D perovskite materials are more stable as compared to 3D perovskite materials under the influence of oxygen, light, and humidity. Attaining high solar cell efficiency and ambient stability simultaneously with a mixed dimensional strategy necessitates a delicate balance in the composition of 2D and 3D perovskite along with the structural motifs for achieving optimized contribution from each of the 2D and 3D perovskite phases. Two major protocols are envisaged for the combination of 2D and 3D perovskites viz. mixed 2D + 3D perovskite, i.e. incorporation of 2D perovskite in bulk 3D perovskite and bilayer 2D/3D thin films, i.e. surface treatment with 2D perovskite phase on a 3D perovskite film. However, depending on the type of synthesis techniques, segregation

of the 2D and 3D perovskite phase in thin films, and type of 2D and 3D perovskite materials, there is a significant influence on the PCE and ambient stability of 2D/3D PSCs.

15.2 Introduction to Perovskite Halides

Gustav Rose in 1839 first coined the term “*perovskite*” for the CaTiO_3 mineral, named after the Russian nobleman and mineralogist Count Lev Alekseyevich von Perovski. Victor Goldschmidt in the year 1926, first used as a general term for describing the crystal structure group (Akkerman et al. 2018). The perovskite crystal lattice is defined as a network of corner-sharing BX_6 octahedra that crystallize with a general ABX_3 stoichiometry (where $\text{A} = \text{CH}_3\text{NH}_3^+$, FA^+ , and Cs ; $\text{B} = \text{Pb}$, Sn , and $\text{X} = \text{I}$, Br or Cl). The standard depiction of the aristo-type cubic perovskite represented either with all the atoms (up) or the BX_6 octahedral network only and the A atoms (down) as depicted in Fig. 15.1a. The typical lattice structure of perovskite material lies in the 3D-perovskite category (Akkerman and Manna 2020). Hybrid perovskites halide were first reported in 1893, but it took around 100 years for researchers to use this material for light-emitting devices and transistors due to their intriguing optical and electronic properties (Shamsi et al. 2019). In the year 2009, the real potential of these materials was tested and discovered for the first time in the field of solar cells (Kojima et al. 2009). Here afterward, the family of PSCs showed promising PCE in a short period.

15.2.1 Dimension-Dependent Types of Perovskite Halides

The dimensionality of perovskite materials engineered by adding/substituting alternative A-site cations, which can modify the 3D perovskite lattice structure either to 2D (layered), 1D (columnar), or 0D (quantum dots) nanostructures. The dimensional-dependent schematic depiction of the crystal structures of perovskite halides to (i) 3D, (ii) layered (2D), (iii) 1D nanorods/nanotubes, and (iv) 0D colloidal nanoparticles is demonstrated in Fig. 15.1b. Among these various nanostructures, this chapter is focused on 2D perovskite halide structures for solar cell applications. Therefore, it is introduced here about the 2D perovskite in detail for the reader’s reference.

Most commonly employed 2D halide perovskite is fabricated by slicing analogous 3D perovskite in the (100) plane, resulting in the formation of 2D perovskites with different numbers of organic layers as depicted in Fig. 15.2. (Ma et al. 2018). Depending upon the type of large chain organic cations selected, 2D perovskites are categorized into three, i.e. Ruddlesden-Popper (RP), Dion-Jacobson (DJ), and alternating cations in interlayer (ACI) (Soe et al. 2018, 2017). Weak van der Waals gaps are observed between each bilayer of monovalent cations and adjacently located two lead halide sheets in the RP-phase 2D perovskites. The difference between the crystal

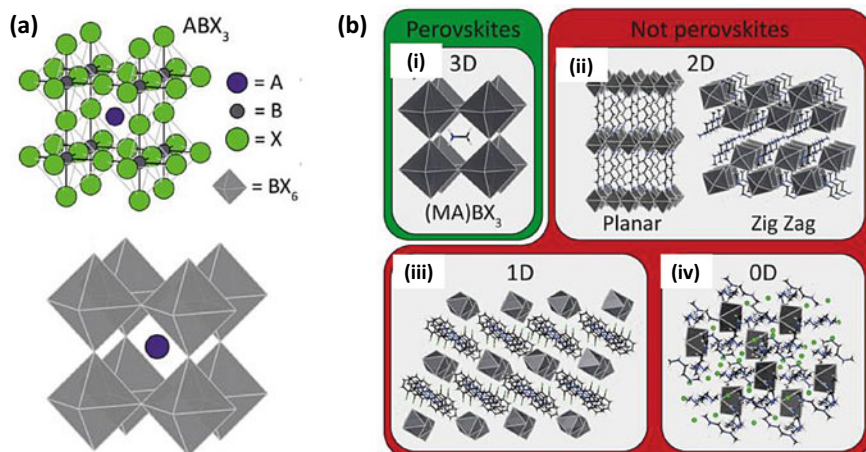


Fig. 15.1 **a** The lattice structure of ABX_3 perovskite structure with two different approaches. **b** Dimensional-dependent classification of perovskite halides into (i) 3D hybrid organic–inorganic metal halides, (ii) Layered (2D) hybrid organic–inorganic metal halides, (iii) 1D metal halides, and (iv) 0D hybrid organic–inorganic metal halides. [reprinted with permission from Akkerman and Manna 2020; Copyright 2020 American Chemical Society]

structures of 3D to quasi-2D to 2D perovskite is shown in Fig. 15.2. The compositions of RP are generally described by $L_2A_{n-1}B_nX_{3n+1}$, (Mao et al. 2018) where L is a long-chain organic cation (spacer) examples include phenyl–ethyl–ammonium (PEA^+) and butylammonium (BA^+), A is a short-chain organic cation that is typically Methyl ammonium ($CH_3NH_3^+$) ion (MA^+), or Formamidinium ($HC(NH_2)_2^+$) ion (FA^+), B is a divalent metal cation like Sn^{2+} or Pb^{2+} , X is a halide anion I^- , Br^- , or Cl^- and n defines the number of inorganic layers held together. Typical PSCs employ 3D ABX_3 structures, where a monovalent “A-site” cation in the cuboctahedral site bonds with the BX_6 octahedra. It is worth noting that when the number of inorganic layers held together $n = \infty$ represents a 3D perovskite, when $n = 1$, it represents the perovskite of pure 2D, and when $n = 2$ to 5, it represents a quasi-2D perovskite. A blend of 3D perovskite and lower-n phases ($n \leq 3$) or higher-n phases ($n = 30$ –60), can lead to the formation of a quasi-3D perovskites (Mei et al. 2014). The parameter “n” in the general formula is equal to the number of octahedral layers. There will be one octahedral layer between two organic layers when $n = 1$. Whereas the inorganic layers contained in this structure behave as a quantum well for the charge carriers while the organic layers act as the barrier (Younis et al. 2021). An alternative to 3D perovskites is quasi-2D perovskites for solar cell application. The quasi-2D perovskites address critical issues of stability faced by the 3D PSCs with high PCE performance. The inspiring achievement sprouted from the developments in the scientific understanding of synthetic chemistry of 2D perovskites and the advancements in the fabrication of stable PSC devices.

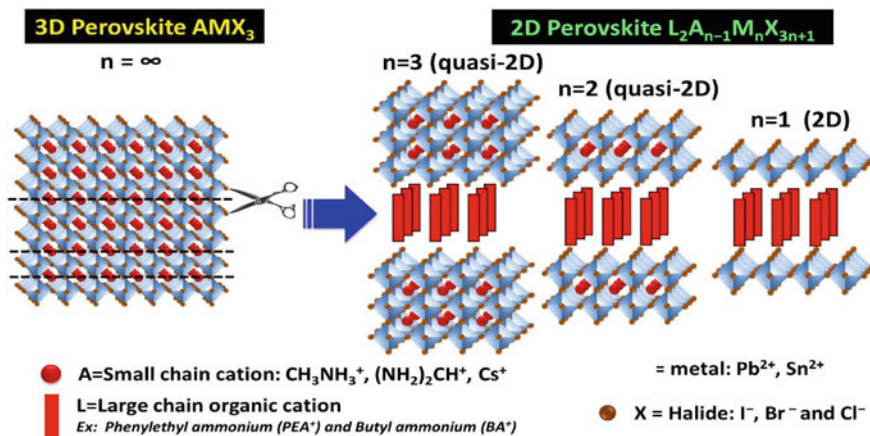


Fig. 15.2 Schematic representation of crystal structure transformation from 3D perovskite to 2D perovskite with the different values of n

15.3 Synthesis of Perovskite Halides and PSCs

Solution-based methods for the deposition of 2D-layered perovskites suffer due to the formation of multiple quantum wells mixtures having a good width (n number) in a random distribution. These factors have substantially hindered the progress in the field of 2D-layered perovskites (Quan et al. 2016; Tsai et al. 2018). Therefore, the deposition of quasi-2D-oriented thin films is still a critical challenge on the thermodynamics of the stability compounds in a solution state.

The perovskite halide materials with 3D, 2D, and mixed dimensional 2D-3D can be synthesized with the most common synthesis process, which is schematically summarized in Fig. 15.3a. They include spin coating, deep coating, screen printing, slot-die coating, and vapor deposition techniques. The hybrid method represents the synthesis method involving intermixing among these techniques. Similarly, the deposition of the electron transporting layer (ETL) and hole transporting layer (HTL) was carried out by deposition techniques including, spin-coating, spray-pyrolysis, hydrothermal, sputtering, and hybrid, which is a combination of these methods. The synthesis methods for the deposition of ETL and HTL are summarized in Fig. 15.3b. In general, perovskite films prepared using vacuum deposition have several advantages such as films with high phase purity, uniformity, pin-hole free and smooth as compared to the films that are processed through solutions. However, this method has disadvantages like a slow deposition process and the requirement of a meticulously controlled vacuum environment. This could be one of the reasons for the few studies reported on the vapor deposition of perovskite and ETL/HTL as compared to the solution processes. As the present chapter is devoted to the engineering of dimensional perovskite halides, the following section covered the synthesis of low-dimensional perovskite in detail. The synthesis protocols for the synthesis of 2D perovskite and

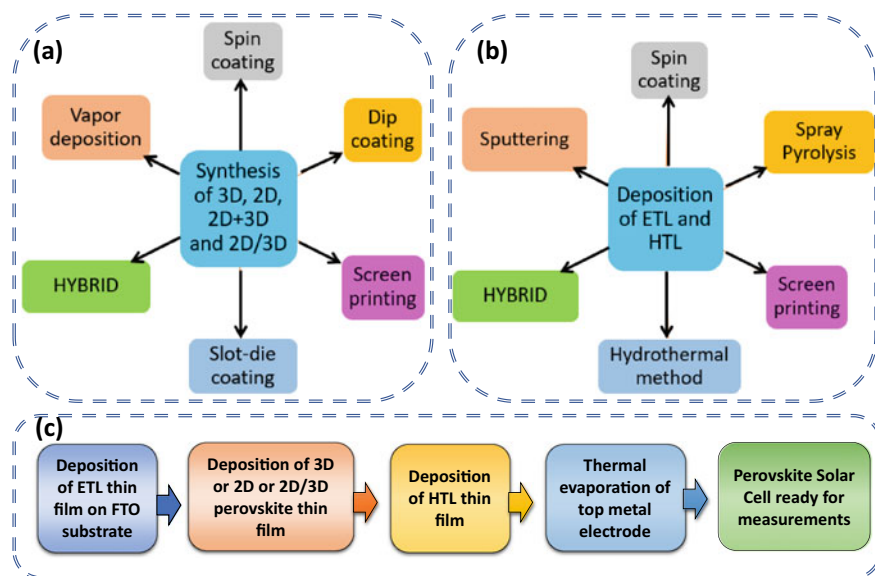


Fig. 15.3 Summary of various synthesis techniques used for the deposition of **a** perovskite halide thin films and **b** electron transport layers (ETL)/hole transport layers (HTL). **c** The important steps involved in the fabrication of perovskite solar cells

different processing strategies for the combination of 2D and or 3D perovskites in PSCs for improved PCE and robust stability are discussed in the following sections.

15.3.1 Synthesis of 2D Perovskite Thin Films

There are several processing strategies by which scientists explore 2D perovskite thin films for application in solar cells. Some of the techniques based on literature are discussed herewith. As demonstrated by Tsai et. al. in $(\text{BA})_2(\text{MA})_3\text{Pb}_4\text{I}_{13}$; where, $n = 4$; (BA = butan-1-ammonium), the 2D perovskites were deposited by hot-casting method (Tsai et al. 2016). In the described method, the initial hot precursor is deposited using a spin-coater on a pre-heated substrate, which is called the hot casting method. They observed that better crystallinity was achieved by hot-casting film at an optimized temperature of 110°C , further confirmed by Grazing Incidence X-ray diffraction (GIXRD) patterns. However, the hot-casting method suffers from reproducibility because of the difficulty in maintaining a uniform temperature for the deposition in large-area substrates. The method is further modified by Zuo et. al. (2019) and demonstrated a process of substrate-heated drop-casting to deposit 2D perovskite. They also achieved the deposition of the 2D perovskite film in large area by developing a method of slot-die coating. A slightly modified method was also proposed by Wu et. al. through slower post-annealing process for the deposition

of the $(\text{BA})_2(\text{MA})_3\text{Pb}_4\text{I}_{13}$; where, $n = 4$ (BA = butan-1-ammonium) 2D perovskite (Wu et al. 2019a). 2D perovskite with structure $(\text{PEA})_2\text{MA}_4\text{Pb}_5\text{I}_{16}$, ($n = 5$) synthesis is reported by Hu et. al. using vacuum poling treatment which resulted in uniform nucleation during crystallization for obtaining the arranged inorganic sheets (Zhang et al. 2019a). The synthesis of $(\text{PEA})_2\text{MA}_4\text{Pb}_5\text{I}_{16}$ perovskite thin films is reported by Gao et. al., which uses a simple spin-coating process. In this method, the growth of highly orientated 2D perovskite films under optimized solvent parameters resulted in improved optoelectronic properties. The optimized solvent composition was (5:5) a mixture of dimethyl formamide (DMF) and dimethyl sulfoxide (DMSO) compared to the film prepared in pure DMF (Gao et al. 2019). Zhang et. al. (Zhang et al. 2017a) explored a single-step spin coating technique for the deposition of a highly crystalline vertically oriented perovskite thin-films of 2D layered $(\text{BA})_2(\text{MA})_{n-1}\text{Pb}_n\text{I}_{3n+1}$ (BA = $\text{CH}_3(\text{CH}_2)_3\text{NH}_3$, MA = CH_3NH_3 , $n = 3, 4$) with the additive, ammonium thiocyanate (NH_4SCN). Further, as lead (Pb) is a toxic element, Cao et. al. (2017) have reported the synthesis of 2D RP $(\text{CH}_3(\text{CH}_2)_3\text{NH}_3)_2(\text{CH}_3\text{NH}_3)_{n-1}\text{Sn}_n\text{I}_{3n+1}$ perovskite using a single step spin-coating method. In brief, the perovskite precursor solution was prepared using 1 mL of DMF over a magnetic stirrer with constant stirring having either 0.2 M of $(\text{BA})_2(\text{MA})_2\text{Sn}_3\text{I}_{10}$ (0.367 g, 0.2 mmol) or 0.2 M of $(\text{BA})_2(\text{MA})_2\text{Sn}_4\text{I}_{13}$ (0.474 g, 0.2 mmol) mixed with 0.2 M of SnF_2 (0.031 g, 0.2 mmol) at 70 °C for 1 h. For the triethylphosphine, 5 μL corresponding to 0.034 M was directly added to the perovskite solution mixture of 1 mL DMF. Spin-coating process for the deposition of the perovskite solution on mesoporous TiO_2 substrates, which was preheated at 120 °C at 3000 rpm for 30 s resulted in the 2D films. The films were then annealed at 75 °C for 5 min. and subsequently allowed to cool to room temperature.

15.3.2 Synthesis of 2D + 3D Mixed Perovskite Layer

The 2D + 3D mixed perovskite layer is also known as the bulk incorporation method. This method involves the incorporation of the spacer organic cationic compounds in the identical precursor solution containing the components of the 3D perovskite (PbI_2 , PbCl_2 , MAI, FAI, CsI, RbI, etc.). This single precursor containing the cations and anions of both 2D and 3D perovskite is spin-coated on the substrate followed by annealing to get the desired thin film of 2D + 3D perovskite phases. Therefore, several parameters like length of organic cation, solvent, concentration, annealing temperature, and annealing time need to be optimized for the high quality of 3D bulk-incorporated 2D perovskite film. A mixed dimensionality perovskite of $\text{BA}_{0.05}(\text{FA}_{0.83}\text{Cs}_{0.17})_{0.95}\text{Pb}(\text{I}_{0.8}\text{Br}_{0.2})_3$ is reported by Wang et. al. with the addition of BA^+ into $\text{FA}_{0.83}\text{Cs}_{0.17}\text{Pb}(\text{I}_y\text{Br}_{1-y})_3$ 3D perovskite (Wang et al. 2017).

A low-pressure vapor-assisted solution deposition process also known as LP-VASP method was applied by Li et. al. for the first time. It was used for the preparation of several 2D/3D hybrid perovskite films. The method uses a low-pressure heating oven to spin coat the substrate with phenyl ethyl-ammonium iodide (PEAI)-doped

lead iodide (PbI_2) followed by a reaction with methyl-ammonium iodide (MAI) vapor. In this process, the authors investigated PEAI/ PbI_2 ratio ranging from 2 to 0 to realize the effect of the ratio of doping PEAI in MAI-vapor-treated perovskites as plays a significant role on the crystallinity, morphology, optical absorption, and the resultant device performance (Li et al. 2018).

In another report, Chen et. al. incorporated 2D PEA_2PbI_4 [$\text{PEA} = \text{C}_6\text{H}_5(\text{CH}_2)_2\text{NH}_3$] in 3D MAPbI_3 [$\text{MA} = \text{CH}_3\text{NH}_3$] fabrication through the Lewis acid–base adduct method. They termed this mixed dimensionality perovskite as $(\text{PEA}_2\text{PbI}_4)_{0.017}(\text{MAPbI}_3)_{0.983}$ thin films. According to the authors, this thin film contains a structure of nanolaminate, which is made up of layered MAPbI_3 nanobricks produced in the presence of 2D PEA_2PbI_4 (Chen et al. 2017). For increasing the stability of α - CsPbI_3 , EDAPbI_4 (EDA = ethylenediamine) was used by Zhang et. al. to obtain 2D perovskite. In this method, authors reported the α - CsPbI_3 is stabilized by the ethylenediamine (EDA) cation using a little amount of 2D EDAPbI_4 perovskite for avoiding the undesirable formation of the non-perovskite phase (Zhang et al. 2017b). Further, deposition of $(\text{MAPbI}_3)_{1-x}[(\text{PEI})_2\text{PbI}_4]_x$ 3D/2D mixed perovskite films through spin coating process is also reported by Yao et. al. (2015). In the two-step deposition, PbI_2 was initially deposited along with precursor solution of PEI-HI (polyethyleneimine hydroiodide) followed by the deposition of $\text{CH}_3\text{NH}_3\text{I}$. The formation of $(\text{PEI})_2\text{PbI}_4$ in the first step lowers crystallization rate of the 3D perovskite and promotes the growth of the 2D perovskite phase among the grains of the 3D perovskite phase. A dip coating with two-step approach was proposed by Koh et. al., which lead to the formation of $(\text{IC}_2\text{H}_4\text{NH}_3)_2(\text{CH}_3\text{NH}_3)_{n-1}\text{Pb}_n\text{I}_{3n+1}$ (Koh et al. 2016). Briefly, the first step involved spin-coating of a pure 2D perovskite ($n = 1$) with a precursor solution containing PbI_2 and $\text{IC}_2\text{H}_4\text{NH}_3\text{I}$ in a particular stoichiometric ratio, which was subsequently followed by the dipping of the substrate in the MAI solution for different time intervals, i.e. varying from 1 min. to 5 min.

Mohite and co-workers in 2016 reported the hot-casting method, which is a new and efficient approach. In the hot casting technique, the substrate consisting of FTO/poly(3,4-ethylene dioxythiophene) polystyrene sulfonate (PEDOT: PSS) was heated at $\approx 150^\circ\text{C}$ before the spin coating process of the perovskite. A superior quality thin film having favored out-of-plane alignment of $(\text{BA})_2(\text{MA})_3\text{Pb}_4\text{I}_{13}$ was achieved (Stoumpos et al. 2017). The authors observed that the PSCs prepared using this method had improved the stability and efficiency of the 2D/3D PSCs.

Grancini et. al. have proposed a method for possible engineering of the interface between the composite of AVA_2PbI_4 2D perovskite and MAPbI_3 3D perovskite halides (Get and al. 2017). Authors prepared 2D-3D perovskite thin films of different compositions through the mixing of different quantities of 1.1 M solution of AVAI: PbI_2 in the ratio of 2:1 and MAI: PbI_2 precursor solution molar ratio of 0, 3, and 5%, respectively. These mixed solution blends are infiltrated in a mesoporous oxide scaffold using a one-step deposition process. The authors observed that the slow drying process allowed the restructuring of the 2D and 3D perovskite phase components in the mixed $\text{AVA}_2\text{PbI}_4/\text{MAPbI}_3$ film before solidification. Finally, according to the authors, a high PCE is obtained for the devices prepared with 3% AVAI perovskite film.

15.3.3 Synthesis of 2D/3D Perovskite Layer

Generally, for the preparation of 2D/3D perovskite bilayers, the two individual precursors containing components of 2D perovskite and 3D perovskite are deposited separately to form individual layers of 2D/3D perovskite thin films. Enhanced stability, a long carrier lifetime, and lower trap density were achieved in 2D perovskite films upon application on the surface of the 3D perovskite film which is further sandwiched to other charge-collecting layers in multi-stacked PSCs (Koh et al. 2018). Spin-coating process of the long-chain alkyl ammonium halides dissolved in isopropanol was used for the deposition at the surface of 3D perovskite film. The presence of water-resistant bulky organic groups at the top of the 3D perovskite films promotes the formation interfacial layer of 2D perovskite for an enhanced stability (Liu et al. 2019a). Deposition of PEA_2PbI_4 2D perovskite film on the top of $\text{Cs}_{0.1}\text{FA}_{0.74}\text{MA}_{0.13}\text{PbI}_{2.48}\text{Br}_{0.39}$ device was achieved by Nazeeruddin et. al. having an efficiency of 20.1% (Cho et al. 2018). The fabricated device had long-term stability as proven after 800 h under the ambient condition at 50 °C sustaining 85% of the initial efficiency. A post-deposition treatment of 3D perovskite by applying an isopropanol solution of penta-fluorophenyl-ethyl ammonium iodide (FEAI) was achieved by Liu et al. (2019b). In another work, the deposition of 2D perovskite film on the top of 3D perovskite film using a mixed solvent o-dichloro benzene and iso-propanol in the 97:3 v/v ratio with n-hexyl trimethyl ammonium bromide (HTAB) as demonstrated by Jung et. al. (2019a). A transparent 2D perovskite deposition on the top of 3D perovskite film was achieved using the dissolution of precursor strategy with alkylammonium bromide dissolved in chloroform by Yoo et. al. (2019). A synthetic approach for the fabrication of a bilayer structure of the type 2D PEA_2SnI_4 along with 3D MASnI_3 perovskite (PEA = phenethylammonium; MA = methylammonium) is reported by Choi et. al. The formation of the bilayer structure was achieved through a sequential vapor process combined with vacuum deposition and followed by vapor reaction. The advantage of the vapor process lies in ensuring the deposition of the uniform upper layer of the 2D perovskite thin film layer without damaging the lower 3D perovskite thin film layer (Choi et al. 2020). But later Joker et. al. (2021) reported a solution processing-based sequential method of deposition using hexafluoro-2-propanol as a solvent for the on the top of the 3D layer deposition of eight bulky ammonium cations to form a 3D/quasi-2D layer preventing the moistures and acting as a protecting layer of the tin perovskite grains.

Yukta et. al. (2022) recently reported the synthesis of 3D MAPbI_3 perovskite passivated by NH_4SCN followed by the deposition of the capping layer of 2D perovskite with organic xylylene diammonium iodide cation. For the deposition of 3D perovskite + NH_4SCN , an adequate amount of NH_4SCN was added to the 3D perovskite precursor solution and stirred for 12 h at 60 °C before use. This mixed precursor solution was spin-coated with chlorobenzene drip @ 1000 rpm for 10 s. and continuously at 6000 rpm for 30 s. which was followed by annealing at

100 °C. For fabrication of a 3D/2D heterojunction, 100 μ L of p-xylylene diammonium iodide/isopropyl alcohol solution was spin-coated on the 3D perovskite + NH_4SCN perovskite surface at 3000 rpm for 30 s and annealed at 100 °C for 10 min.

The synthesis of 2D-3D graded perovskite was reported by Garai et al. (2021). The 2D-3D graded perovskites use a multifunctional 4-(aminomethyl)benzoic acid hydrogen bromide (ABHB) molecule synthesized strategically for the treatment surface in the fabrication process. Briefly, MAPbI_3 precursor solutions consisting of dissolved MAI and PbI_2 in 1:1 ratio in a mixed solvent system containing Gamma butyrolactone (GBL)/Dimethyl Sulphoxide (DMSO) (7:3, v/v) were spin-coated at 750 rpm for 20 s and 4000 rpm for 60 s with 160 ml anhydrous Toluene dripped after 20 s as antisolvent and annealed at 80° C for 10 min. Different concentrations of ABHB solution in isopropanol containing 1, 2, and 3 mg/mL were spin-coated at 4000 rpm for 30 s above the perovskite layer. The ABHB-treated perovskite film was annealed further at 80° C for 5 min. This could effectively form 2D perovskite thin film over MAPbI_3 3D perovskite thin films for solar cell applications.

With the above examples, it can be concluded that different processing approaches are used for only 2D, 2D + 3D mixed, and 3D/2D bilayer perovskite thin film depositions for solar cell applications. However, it has been observed that in all these types of thin films, the growth of 2D and 3D perovskite is different, and an in-depth analysis of growth mechanisms needs to be explored. This is because synthesis techniques play a key role in the formation of perovskite layers with different crystal structures, different lattice orientations, and the distribution of 2D and 3D perovskite material. All these changes in the perovskite thin films affect the charge transport mechanism and in turn, decide the photovoltaic performance of the solar cell devices. It is also important to note that the synthesis is also sensitive to the type of initial precursors like the size of organic cations, additives, solvents, humidity, and substrate temperature.

15.4 Fabrication of PSCs with Different Perovskite Phases

The in-depth procedure for the fabrication of a general perovskite solar cell is elaborated as follows. The important steps involved during the fabrication of perovskite solar cells are schematically depicted in Fig. 15.3c. The step-by-step process for fabricating perovskites solar cells is discussed herewith. Zinc metal powder and 2 M HCl were utilized for etching FTO-coated glass substrates followed by washing with deionized (DI) water. Further, the etched substrate was subjected to ultrasonic cleaning using detergent, DI water, acetone, and ethanol, which was then dried finally using dryer. The hydrophilicity of the substrate surface was enhanced by UV-ozone treatment for a few minutes. The electron transporting material (ETM) can be deposited with any suitable method mentioned in Fig. 15.3. In general, techniques like spin-coating and/or spray-coating followed by annealing of thin films were used to deposit ETM thin films. The popular metal oxide-based electron transporting materials are TiO_2 , SnO_2 , and ZnO (Haque et al. 2017), whereas (Gangadharan and Ma

2019; Gangadharan and Ma 2019)-phenyl C61 butyric acid methyl ester (PCBM) (Xiao et al. 2014), C60 and their derivatives (Liang et al. 2014) have been used as n-type type charge carriers. In the next step, depending upon the type of perovskite materials, a precursor solution discussed in the previous section needs to be prepared separately. This precursor solution can be deposited on the ETM layer-coated FTO substrates. Here, note that depending upon the type of perovskite thin film, i.e. pristine 2D, pristine 3D, mixed 2D + 3D, or 2D/3D bilayer thin films, the precursor solution can be prepared as discussed in the above sections. Again, the perovskite layer can be deposited with any solution processing techniques or physical vapor deposition methods discussed in the above sections. This perovskite layer is required to deposit in the inert and controlled humidity conditions, which were found in the glove box. The fabrication of high-quality perovskite thin films depends on many processing parameters and hence is highly sensitive to the photovoltaic performance of perovskite solar cells. The various methods investigated in the literature for 2D, 2D + 3D, and 2D/3D perovskite layers have been discussed in this chapter later.

Next, the perovskite layer was covered by the deposition of the HTL, which could consist of either organic or inorganic materials. The most common way of deposition of HTL is again the spin coating technique for all types of organic materials. For inorganic materials, physical vapor deposition techniques were also used. One precaution required to take during the HTL deposition is to protect the perovskite thin film layer. The most efficient and widely used organic hole transport materials are poly(3,4-ethylenedioxythiophene) polystyrene sulphonate (PEDOT:PSS) (Xiao et al. 2014; You et al. 2014), 2,2',7,7'-tetrakis(N,N-pdimethoxyphenylamino)-9,9'-spirobifluorene (spiro-OMeTAD) (Sheikh et al. 2015, 2017, 2019), poly[bis(4-phenyl)(2,4,6-trimethylphenyl)amine] (PTAA) (Jeon et al. 2014b; Yang et al. 2015), and poly(3-hexylthiophene-2,5-diyl) (P3HT) (Conings et al. 2014) in PSCs. Finally, metals like gold or silver thick layers were deposited using the thermal evaporator on the top of HTL, which acts as the top electrode.

In the early work, the device design of PSCs is based on solid-state DSSCs. The two most promising device architectures include mesoporous electron transporting layer-based PSCs and planar PSCs, which were initially focused on the optimization of the efficiency of the PSCs. In mesoporous perovskite solar cells, the mesoporous (scaffold) layer of inorganic metal oxides like TiO_2 , Al_2O_3 , SnO_2 , SrTiO_3 , etc. was deposited on a FTO substrate with a compact TiO_2 thin film-coating. The perovskite layer was deposited on this mesoporous layer followed by the HTL layer. In the case of planar perovskite solar cells, the perovskite thin film was deposited directly on the compact TiO_2 thin film-coated FTO substrate followed by deposition of the HTL layer. More details about the device architecture can be found in a recent review article (Ge et al. 2020).

This part is focused on the dimensional engineering of the perovskite layer and its impact on the performance of the device and ambient stability. It was observed from the literature that researchers explored various combinations of 2D and 3D perovskite materials for optimizing the device performance with higher stability. Some of the most common device architectures are schematically represented in Fig. 15.4, which will be discussed in this chapter. As observed apart from 3D perovskite, 2D, 2D

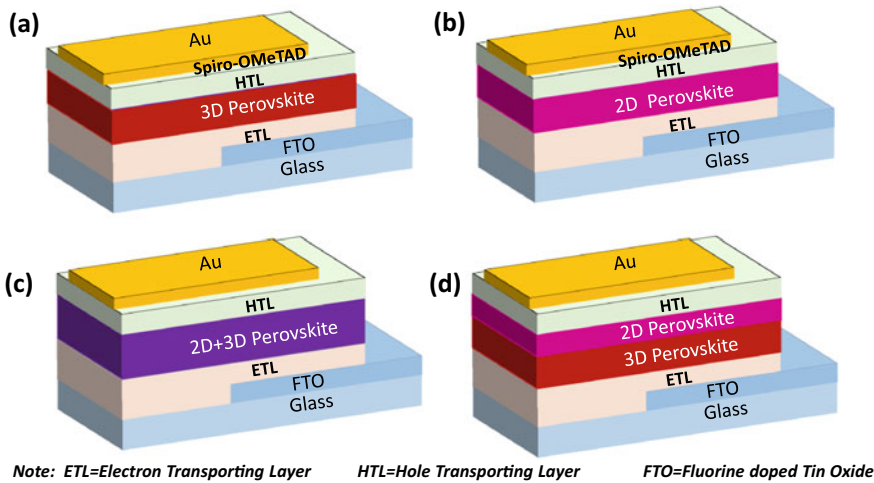


Fig. 15.4 Schematic representation of the device structure for **a** 3D perovskite solar cell, **b** 2D perovskite solar cell, **c** 2D + 3D mixed perovskite solar cells, and **d** 2D/3D layered perovskite solar cells

+ 3D mixed perovskite, and 2D/3D layered perovskite-based solar cells have been fabricated and tested in the literature. As denoted in Fig. 15.4, only the perovskite thin film with its different dimensional phases has been changed and all other layers are required to complete the solar cell device. The photovoltaic properties of the PSCs having a similar structure shown in Fig. 15.4 are discussed in the section below.

15.5 Photovoltaic Properties of 3D, 2D, 2D + 3D, and 3D/2D-Based PSCs

The following section has reviewed the recent work on the key issues that affect enormously the performance of 3D, 2D, 2D + 3D, and 3D/2D perovskite-based solar cells. First, the device configuration structures and properties of 3D, 2D, 2D + 3D, and 3D/2D perovskites will be introduced briefly and the photovoltaic performances are summarized.

15.5.1 3D Perovskite Halide-Based Solar Cells

The journey of hybrid perovskite halide-based solar cells has started with the 3D perovskite halide materials for sunlight harvesting due to their excellent optoelectronic properties. The first report on 3D PSCs has been published by Miyasaka and

co-workers in the year 2009 with modest PCE of 3.8% (Kojima et al. 2009). As a breakthrough in the field was observed when the PCE of PSCs was improved from 10 to 20% in a short period (Saliba et al. 2016; Li et al. 2016). Over the past few years, PSCs have undergone a miraculous journey, showing continuous and rapid progress the PCE of PSCs reached a recent record value of 25% (Green et al. 2020). This indicates that the PCE achieved in 3D PSCs, which are competing with the commercial silicon solar cells. However, the PSC technology faces the most crucial issue of ambient long-term atmospheric instability. In addition to solar cells, the perovskite halides have shown promising applications in light-emitting diodes (Kim et al. 2022), photocatalysis (Deshpande et al. 2021), and gas sensors (Sheikh et al. 2022; Bhosale et al. 2023).

Several attempts (Sheikh et al. 2015, 2017; Ugur et al. 2017; Haque et al. 2017) to explore the impact of atmospheric moisture, atmospheric oxygen, atmospheric UV light, and temperature have been made for understanding the degradation of PSCs. Despite the innovations for improving PSC stability under various environmental conditions, the stability of 3D perovskite halide materials against moisture and temperature is still the focus of researchers working in the area of PSC development.

15.5.2 2D Perovskite Halide-Based Solar Cells

According to recent studies, the 2D perovskite halides have higher ambient condition stability as compared to those 3D perovskite halides. The presence of bulky organic spacer in the 2D perovskite structure contributes to more hydrophobicity. Further, highly oriented lattice structures and compact packing density lead to the reduction in the grain boundary density, minimizing the direct contact of water molecules with the 2D perovskite layer. (Ortiz et al. 2019) In addition to this, the layered 2D perovskites structure shows higher thermal stability and larger cations hamper internal ionic motion which further improves the stability (Smith et al. 2014a). However, the wide optical bandgaps and limitations in the charge transport of the 2D perovskites, the 2D perovskite-based solar cell shows limited performance. The PCE of 2D perovskite material is required to be enhanced compared to the performance of 3D perovskite-based solar cells. The multi-functional role of the 2D perovskites in a solar cell is as a capping layer, as a passivating layer, as a prime cell absorber and as an absorber in the hybrid 3D/2D perovskite-based solar cells. Recently, the production by a spatially disconnected 3D structure with a “protective” species, incorporation of emerging 2D-layered perovskites, provides a promising solution to the environmental stability issue of 3D PSCs (Gangadharan and Ma 2019). Therefore, 2D-layered metal-halide perovskites have generated the highest research interest and as one of the best materials for the fabrication of long-term, operationally stable with high-performance PSCs because of their desirable optoelectronic properties (Quintero et al. 2018; Zhou et al. 2017).

The most relevant works of literature on the fabrication of 2D/quasi-2D PSCs are tabulated in Table 1. Some significant points are briefly summarized as follows. The

first quasi-2D perovskites ($\text{PEA}_2\text{MA}_2\text{Pb}_3\text{I}_{10}$) were demonstrated by Karunadasa et al. in mesoscopic PSCs with an efficiency of 4.73% in 2014 (Smith et al. 2014b). A hot-casting method by Tsai et al. was the first method reported for the preparation of 2D perovskite $(\text{BA})_2(\text{MA})_3\text{Pb}_4\text{I}_{13}$ ($n = 4$), achieving a PCE = 10% for the first time (Tsai et al. 2016). Zuo et al. have achieved a PCE of 14.9% for the solar cell based on self-assembled 2D $(\text{BA})_2(\text{MA})_3\text{Pb}_4\text{I}_{13}$ perovskite films with uniform and oriented, deposited using the drop-casting method on hot substrates (Zuo et al. 2019). A slow post-annealing process was proposed by Wu et al. for the deposition of $\text{BA}_2\text{MA}_3\text{Pb}_4\text{I}_{13}$ -based 2D PSCs having PCE of 17.26%, a favorable bandgap energy alignment within the 2D perovskite was achieved owing to the vertical distribution of different perovskite phases in gradient (Wu et al. 2019b). According to the authors, these slow post-annealing processed devices exhibit satisfactory stability with less than 4.5% of degradation after 2000 h in N_2 environment without encapsulation. Similar efforts have been carried out to improve the performance and stability of 2D PSCs (Cheng et al. 2018; Lai et al. 2018; Yao et al. 2016). Another strategy reported by Zhang et al. uses vacuum poling treatment for arranging variable- n -value nanoplates, enforcing homogenous nucleation in the process of crystallization (Zhang et al. 2019b). This approach yielded $(\text{PEA})_2\text{MA}_4\text{Pb}_5\text{I}_{16}$ -based PCE of 18.04%. As observed different reports focused on various growth mechanisms of 2D perovskite and observed different PCE values. Thus, insight mechanistic studies of the crystallization process of hot-casting or solvent processing are emphasized for deeper understanding (Zhang et al. 2020). Soe et al. (Soe et al. 2018) reported deposition of highly oriented 2D RP perovskite $(n\text{-butyl-NH}_3)_2(\text{MeNH}_3)_4\text{Pb}_5\text{I}_{16}$ thin films from dimethyl formamide/dimethyl sulfoxide mixture solvents using the hot-casting method. As per the data, the PSC prepared with this method shows a PCE of 10% with an open-circuit voltage of ≈ 1 V. The photovoltaic devices based on $(\text{BA})_2(\text{MA})_2\text{Pb}_3\text{I}_{10}$ and $(\text{BA})_2(\text{MA})_3\text{Pb}_4\text{I}_{13}$ perovskite using the precursor's BAI: methylammonium iodide: PbI_2 : NH_4SCN molar ratio composition of 2:2:3:1 showed average PCE of 6.82% and 8.79%, respectively, as reported by Zhang et al. (2017a). Both the devices without shielding performed with excellent stability with a constant PCE during the time span of the storage in a glove box purged with purified N_2 . The lead-free 2D perovskite-based PSCs were reported by Cao et al. (2017), however, the PCE is found to be 2.5% and needs more investigation to further increase the PCE.

According to Liang et al. and co-workers (Liang et al. 2021), the 2D thin films deposited using the conventional halide spacers result in thin films having a mixture of random well with width (n number) distribution and multiple quantum wells, which are treated as multi-quantum wells (MQWs). They have designed a strategy that can deposit phase-pure metal-halide perovskite quantum wells (QWs), which have highly oriented lattices. The schematic representations of the structure of the multi-phase and the pure-phase 2D perovskite film are shown in Figs. 15.5a, b, respectively. Figure 15.5c, d shows the XRD patterns of the pure phase 2D perovskite film deposited using BAI and BAAC, respectively. In multi-phase 2D perovskite film deposited using BAI, clear periodic 2D crystallographic planes (001) and (010) are observed for $n = 1$ and $n = 2$ film, respectively. However, according to the

authors, for the largely mixed-phase films with $n \geq 3$, the 2D crystallographic planes disappear. In contrast, all the deposited films having $n = 2, 3, 4, 5$ with BAAC show a clear periodicity of the 2D crystallographic planes ($0k0$), which confirms the high phase purity. The authors analyzed surface morphologies of the films, which were characterized using SEM as shown in Fig. 15.5e, f. These results indicate to obtain, smooth surface having a controlled large average grain size of $\sim 10 \mu\text{m}$ a phase-pure QW films should be used, while for smaller grains of $\sim 1\text{--}2 \mu\text{m}$ and recognizable pinholes, the MQW films should be used. A cross-sectional SEM demonstrates the architecture of the device: ITO/SnO₂ ($\sim 50 \text{ nm}$)/layered perovskite ($\sim 500 \text{ nm}$)/spiro-OMeTAD ($\sim 200 \text{ nm}$)/MoO₃ ($\sim 5 \text{ nm}$)/Au ($\sim 80 \text{ nm}$) is shown in Fig. 15.5g. The J-V characteristics of the best-performing PSCs are shown in Fig. 15.5h. As observed the PCE of the phase pure QW-based PSC and the MQW-based PSC, as 16.25% and 13.81%, respectively. Further authors claim that these solar cells are stable for $4,680 \text{ h}$ after keeping at $65 \pm 10\%$ humidity. Only less than 10% efficiency degradation was reported after keeping them for 1100 h in a continuous light illumination condition.

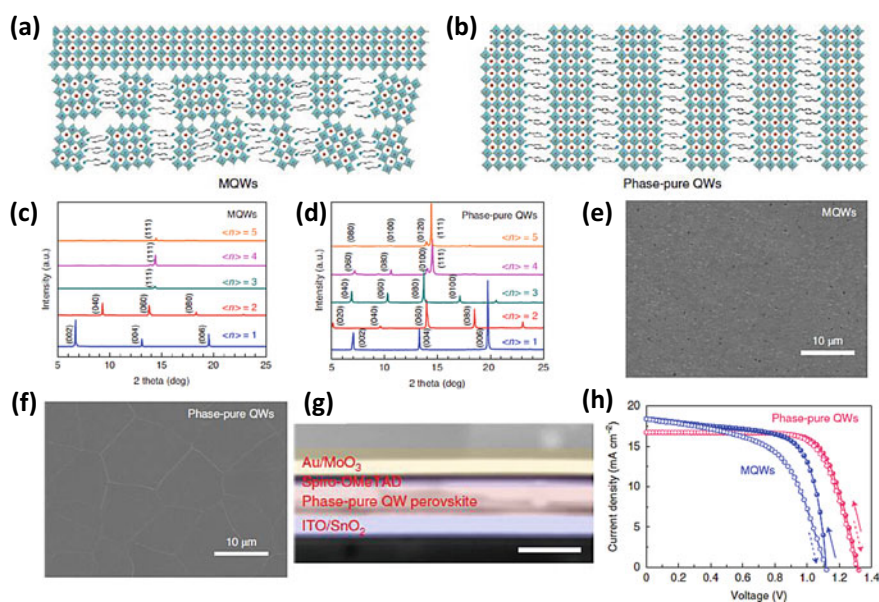


Fig. 15.5 Schematic structure of the multi-phase (a) and the pure phase (b) 2D perovskite film. The XRD patterns of the multi-phase (c) and pure phase (d) 2D perovskite films. The SEM images of the multi-phase (e) and pure phase (f) 2D perovskites thin films and (g) cross-section SEM image showing the device architecture. (h) Comparative current density vs voltage measurements of the best-performing PSCs with multi-phase and the pure phase 2D perovskite film. (Reprinted with permission from Ref. 79; Copyright 2020 Springer Nature)

15.5.3 Halide-Based 2D/3D Perovskite Solar Cells

The 3D perovskite-based solar cell is more advantageous than the 2D perovskite-based solar cell. The 2D perovskite-based solar cell shows a lower efficiency as a result of hindrance in the charge carrier transport because of the presence of bulky organic cations in the crystal structure. On the other hand, the highly efficient 3D perovskite solar cell suffers from low environmental stability. The incorporation of 2D perovskite into the 3D perovskite structures together can lead to balancing of the problems of a solar cell device, i.e. stability and efficiency (Krishna et al. 2019; Manjunath et al. 2022; Kim et al. 2021). The integration of 2D and 3D perovskite can be done in two main types either by blending/mixing the precursors of 2D and 3D or by layer-by-layer sequential method of deposition to obtain an engineered 2D/3D bilayer structure. The progress of combining 3D perovskite and 2D perovskite strategies reported in the literature has been explored in the following sections.

15.5.3.1 2D + 3D Perovskite-Based Solar Cells

The disadvantage of 2D perovskite as compared to 3D perovskites is the limitation in the performance of pure 2D perovskite-based solar cells. Some of them are mentioned herewith. After the transformation of 3D perovskite to 2D perovskite, the organic spacers used in such solar cells, form thin insulating layer sandwiched between the two slabs of conductive metal halide, leading to a reduction in conductivity of the current in the 2D perovskite films and impedes the extraction of charge as compared to 3D perovskites. Similarly, in comparison to 3D perovskite, 2D perovskite has a relatively higher optical band gap (≈ 2.5 eV), which requires a shorter spectral range for light absorption. Also, the binding energy of 2D perovskite is higher than that of 3D perovskite. Therefore, to overcome these issues of 2D perovskite, mixed 2D-3D or 2D + 3D perovskite films are preferable for fabricating PSCs, which could offer both high photovoltaic performances from 3D perovskite and superior device stability due to 2D perovskite.

In 2014, mixed 2D/3D multidimensional perovskite-based PSCs were conceptually achieved for the first time by Smith et. al. wherein MA cations were mixed with a large amount of PEA to produce a Ruddlesden–Popper structure with a composition: $(\text{PEA})_2(\text{MA})_2[\text{Pb}_3\text{I}_{10}]$ (Smith et al. 2014a). Despite the low PCE of 4.73%, the mixed 2D + 3D perovskite of $(\text{PEA})_2(\text{MA})_2[\text{Pb}_3\text{I}_{10}]$ composition-based device showed a high V_{oc} of 1.18 V. The work also achieved long-term stability of 46 days of air exposure subjected to relative humidity (RH) of 52%, for the 2D/3D mixed perovskite film while the PSCs prepared with MAPbI_3 completely degraded. Li et. al. (2018) proposed a device that consists of FTO/C-TiO₂/m-TiO₂/PEAI-MAPbI₃/Spiro-OMeTAD/Ag prepared with the LP-VASP method. In this device, according to the authors, it is proposed the MAPbI₃ perovskite grain is surrounded by the PEAI-containing perovskite grain, which improves their grain growth. The fabricated device based on $(\text{PEAI}/\text{PbI}_2 = 0.05)$ was able to achieve the PCE of 19.10%

with a J_{sc} of 21.91 mA/cm², V_{oc} of 1.08 V along with an excellent fill factor (FF) of 80.36%. However, the authors have not reported their ambient device stability. Similarly, Hu et. al. used an antisolvent engineering method for the PEA incorporation in the 2D/3D Pb–Sn alloyed perovskite solar cell and observed the highest PCE of 15.93% for the device of 2D/3D PEA_xMA_{1-x}Pb_{0.5}Sn_{0.5}I₃ (Zhang and Hu 2020).

Koh et. al. reported a perovskite solar cell based on 2D + 3D perovskite with excellent stability in the air at a controlled relative humidity of 70–80% for both encapsulated and non-encapsulated are observed for the perovskite thin films obtained within 5 min. of dipping time. An outstanding 9% (J_{sc} = 14.88 mA/cm², V_{oc} = 0.883 V, and fill factor (FF) = 0.69) power conversion efficiency under AM 1.5G condition was achieved (Koh et al. 2016). Stoumpos et. al. reported a solar cell device in which hot casting of (BA)₂(MA)₃Pb₄I₁₃ was done on PEDOT: PSS coated FTO substrate (Stoumpos et al. 2017). This work demonstrated a major advancement in the device PCE of 12.5% for the first time. The 2D material incorporation for stability is also validated in this work, as the non-encapsulated device fabricated using a mixed-dimensional perovskite was found to retain 60% of the initial efficiency up to 2250 h at room temperature in a continuous incident light exposure condition. Further, this work also reports an improved tolerance to 65% relative humidity compared to 3D perovskites.

Grancini et. al. reported a highly stable and robust device based on mixed 2D (HOOC(CH₂)₄NH₃)₂PbI₄ and 3D CH₃NH₃PbI₃ perovskite thin films (Get and al. 2017). A schematic representation of PSC with and without HTM is shown in Fig. 15.6a. As observed authors prepared one device consisting of regular spiro-OMeTAD-based HTL followed by the metal electrode and in the other PSC device the conducting carbon was used, which works as an efficient hole transporting layer and no need for the metal electrode. Figure 15.6b shows the J-V plot and characteristics of 2D/3D perovskite solar cell with an optimized 3% AVAI mixture and Spiro-OMeTAD/Au. The device with HTM shows PCE of 14.6% for mixed 2D/3D perovskite and 15% for 3D perovskite thin film. The comparative time-dependent variation of normalized PCE of the PSC devices with standard 3D and with the mixed 2D/3D perovskite is shown in Fig. 15.6c. The PSCs with mixed 2D/3D perovskite exhibit a better performance in the stability of the device as compared to the pristine 3D CH₃NH₃PbI₃ cells as observed in Fig. 15.6c. The stability study carried out by the authors indicated the PCE of mixed 2D/3D perovskite halide achieved 60% of the initial value in argon atmosphere even after 300 h of continuous illumination and is more stable as compared to the standard 3D perovskites. Further, the PCE of PSC prepared with this optimized mixed perovskite in a carbon-based architecture observed a yield of 12.9% efficiency. The authors demonstrated the up-scaling by fabricating a solar module of the dimension 10 × 10 cm² using an industrial-scale printable process. The solar module delivered 11.2% efficiency and a stability of 410,000 h. Further, it observed under controlled standard conditions a zero loss in the performances as shown in Fig. 15.6d.

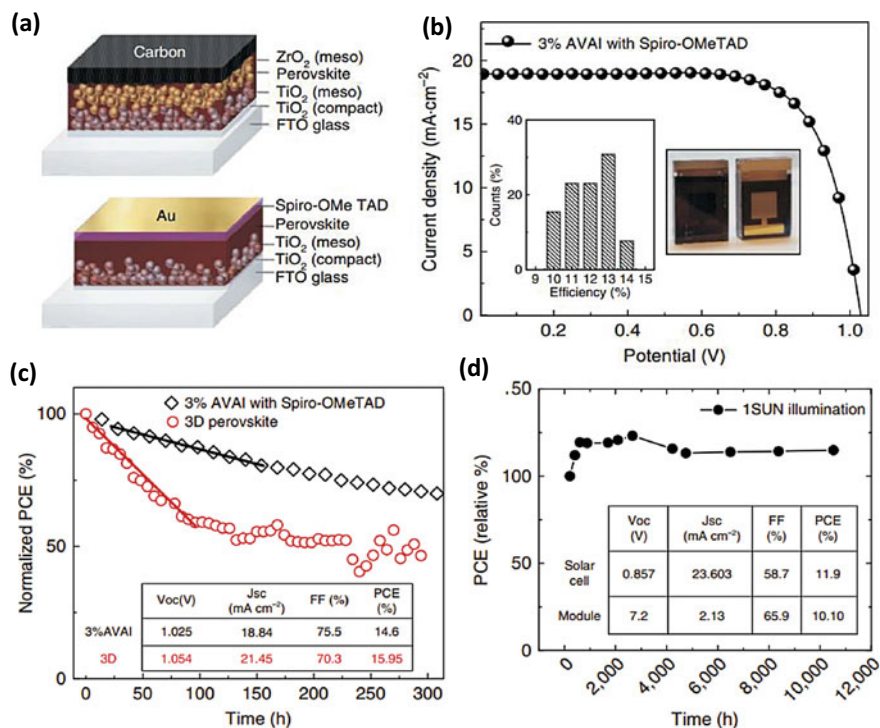


Fig. 15.6 **a** Schematic representation of PSC with and without the HTM **b** J-V curves for the 2D/3D PSCs with 3% $HOOC(CH_2)_4NH_3I$, AVAI hereafter, with device statistics and picture of the cell in the inset. **c** Comparative stability curves of PSCs with the standard 3D and the mixed 2D/3D perovskites. **d** Typical module stability test under 1 sun AM 1.5 G conditions at a stabilized temperature of 55 °C and short circuit conditions. [Reprinted with permissions from Ref. 44; Copyright 2017 Springer Nature under Creative Commons License]

15.5.3.2 2D/3D Bilayer Perovskite-Based Solar Cells

In this strategy, the 2D perovskite layer was deposited over the top of a 3D perovskite layer, which ultimately protects the 3D perovskite from moisture. This section elaborated on recent work so far conducted on 2D/3D bilayer perovskite-based solar cells.

As developed by Cho et. al. (2018), a two-step deposition method was used to fabricate perovskite solar cells of 3D $MAPbI_3/2D \text{ PEI}_2PbI_4$ bilayers (Grancini and Nazeeruddin 2019). The dynamical spin deposition of isopropanol solution of PEAI over the mixed halide 3D perovskite with excess PbI_2 induced layer-by-layer growth. Segregation of the excess PbI_2 was observed over the top of the 3D perovskite. Thus, the in-situ reaction of PEAI with PbI_2 at the top surface leads to the deposition of a thin layer of 2D on the top of the 3D layer. Thus, the 2D perovskite lies at the interface with the hole transporting material (HTM) forming the top surface which reduces the

interfacial charge-carrier recombination leading to the rise PCE over 20%, which is retained even after 800 h exposure at 50 °C using 1 Sun illumination under suitable environmental conditions. Significantly, these results provide encouraging developments toward achieving significantly improved stability without compromising the PCE. Further, the base surface of n-i-p devices architecture can be developed using 2D perovskite anchored on the TiO₂ surface. In a recent development, an ultrathin wide-bandgap halide (WBH) was used to achieve a double-layered halide architecture by Jung et. al., i.e. 2D perovskite halide stacked on a narrow band-gap light absorbing halide layer resulting in a 3D perovskite halide, prior to HTM deposition. The insertion of the WBH layer was found to effectively reduce the charge recombination at the interface of perovskite and P3HT. Therefore, an enhanced PCE of around 23% with long-term (1370 h) operational stability with 1 Sun illumination with 95% of the initial efficiency at room temperature was achieved (Jung et al. 2019b).

Garai et. al. (2021) reported the 2D ABHB-3D MAPbI₃ graded perovskite heterostructure-based perovskite solar cells. The authors observed that after precise treatment with ABHB, the surface of MAPbI₃ 3D perovskite converted into a superior quality 2D/3D perovskite heterojunction film with a reduced grain boundary and better surface coverage. The ABHB-dependent variation in the J-V characteristic of the solar cell is shown in Fig. 15.7a. A PCE of 15.14% was observed for the device without modification while the device after 2 mg/mL ABHB treatment shows improved efficiency of 21.18%. The reproducibility of the process was checked with 15 fabricated devices using the process and plotting of all the parameters of the device in the form of a box chart. The histogram plot, Fig. 15.7b shows the optimum distribution of the device parameters for 15 individual cells with and without ABHB treatment. The images of the films with and without ABHB treatment captured by FESEM are shown in Fig. 15.7c, d. From the images, it was observed that ABHB treatment helps to improve the average grain size and compactness of the thin film morphology. Therefore, better surface coverage, higher quality perovskite films with a reduction in the grain boundary are achieved by ABHB treatment. These factors are responsible for the increase in the PCE of ABHB-treated films as compared to pristine films. In addition to this, the authors claim the role of carboxylic acid and amino groups for effective reduction in the trap states while the halide vacancies are filled by the bromide ions incorporated into the perovskite lattice of 3D MAPbI₃ thin film surface. This type of 2D-3D perovskite-based solar cells is able to minimize effectively the carrier recombination, enhances charge transport and a higher generation rate as compared to pristine 2D or 3D perovskite-based solar cells. As expected, the 2D layer on top devices showed improved stability in ambient conditions owing to better hydrophobicity as shown in Fig. 15.7e. Finally, the device stability was measured by authors for PSCs with and without treatment of ABHB measured at different time spans as shown in Fig. 15.7f. The storage of the devices was maintained at room temperature at a relative humidity range of 40–50%. The improved environmental stability was co-related with the hydrophobicity of the ABHB-treated perovskite.

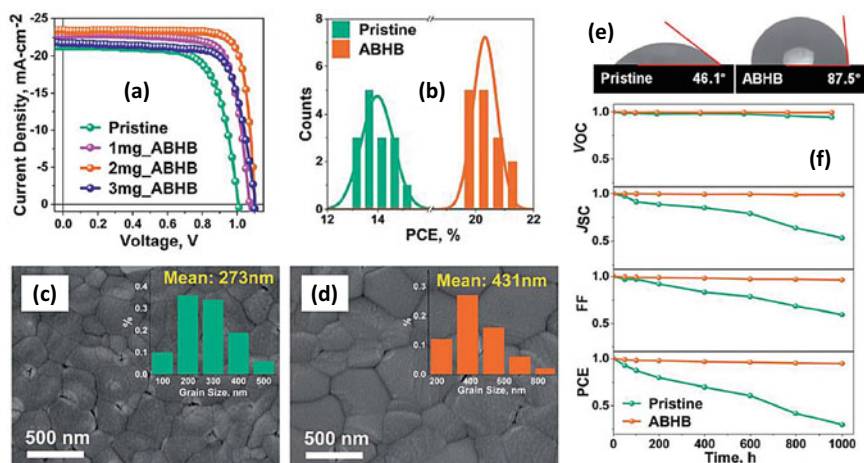


Fig. 15.7 a J-V curves, b histogram, c, d SEM images of pristine and varying concentrations of ABHB treated devices, e measured contact angle of pristine and ABHB treated films, f time-dependent normalized V_{oc} , J_{sc} , FF and efficiency of pristine and ABHB modified devices. (Reprinted with permission from Ref. 87; copyright 2021 The Royal Society of Chemistry)

The NH_4SCN passivated 3D MAPbI_3 perovskite active layer with a further 2D perovskite capping layer using xylylene diammonium iodide organic cation thin films was used for the fabrication of perovskite solar cells by Yukta et. al. (2022). The NH_4SCN passivated MAPbI_3 perovskite-based solar cell device has shown 19.6% PCE, which is higher as compared to pristine MAPbI_3 perovskite solar cells (PCE = 17.18%). Further, the author reported the highest PCE of 20.74% for the 2D/3D perovskite heterojunction-based solar cells. According to the authors, reduced defect density and most significantly inhibition of losses due to nonradiative recombination attributed to the improved PCE of the 2D/3D PSCs. Additionally, the exceptional ambient stability of the as compared to pristine 3D perovskite-based PSCs is because of the hydrophobic 2D capping layer on the 2D/3D heterojunction perovskites. The above discussion identifies that the top 2D perovskite layers improve the surface robustness of the 3D perovskite layer by passivating the surface defects, inducing hydrophobicity, and reducing surface charge recombination (Bouduban et al. 2019). This improvement could ultimately improve the photovoltaic performance of the 2D/3D perovskite-based solar cell devices.

15.6 Conclusions

In conclusion, the present chapter provides in-depth knowledge about the fundamental concepts of not only perovskite solar cells but also to engineer the perovskite materials at mixed dimensionality successfully. This chapter explored the introduction to dimensional-dependent structural properties of perovskite halides. The various synthesis methods explained how to prepare the devices with different solar cell device architectures. The summary of the chapter is schematically illustrated in Fig. 15.8. This figure indicates that the 3D perovskite halide materials are most promising to provide high efficiency but are highly sensitive to environmental parameters. As a result, as far as commercialization of the 3D PSC-based technology, there is no balance of PCE and stability (Fig. 15.8a). Further, by reducing the 3D perovskite to 2D perovskite, the properties of the 2D materials get changed significantly. Moreover, there is a significant increase in the band gap and exciton binding energy due to which pristine 2D-based PSC performance is limited. However, the large organic spacers in the 2D perovskite allow higher hydrophobic surface, which makes them more robust compared to 3D perovskite. This is schematically presented in Fig. 15.8b, where, the stability of the 2D perovskite gained more weight compared to its PCE performance. The mixed halide strategy provides a promising opportunity where the balance between the ambient stability and PCE of the PSC could be obtained. As depicted in Fig. 15.8c, the combination of 2D and 3D perovskite could synergistically provide high efficiency and high stability.

Overall present chapter attracts the attention of readers towards dimensionality tuning of the perovskite in particular the low-dimensional perovskites with greater stability against moisture as compared to their standard three-dimensional native

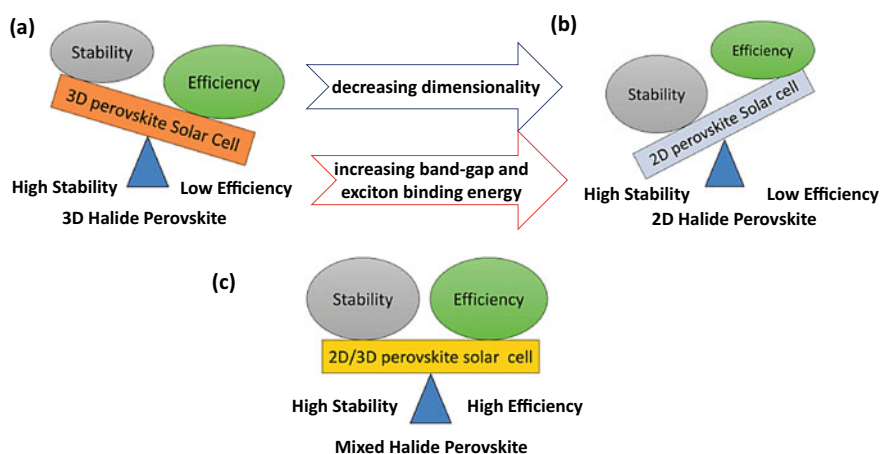


Fig. 15.8 Graphical Illustration of the summary of the PCE and stability of perovskite solar cells prepared with **a** pristine 3D, **b** 2D, and **c** mixed-dimensional 2D/3D perovskites

structures. Thus, a deeper understanding of the fundamental relationship of structure–property of different 2D perovskite phases in combination with 3D perovskite phases is necessary for developing new strategies to design and fabricate a durable, high-performing photovoltaic device. The diversity in the composition of 2D perovskites along with property-dependent choice of novel organic spacer cations provides a huge scope for further scientific exploration. Understanding the mechanism of the organic spacer cations influencing the structures and properties relationship of the 2D perovskites is the necessary step in the advancement of designing better materials for high performance with decisively high stability for optoelectronic applications. The investigation of novel HTLs for inverted PSCs could influence leading to a wider range of new developments with significant improvements in the device performances. Moreover, the proposed studies based on the development and optimizations of novel materials remain important to use cost-effective HTLs for further improvement in the stability of the quasi-2D PSCs.

It has been observed that the robustness of 2D PSCs is higher but has limited PCE. However, the dimensional engineering of perovskite materials plays a multi-functional role in the field of solar cells, like the capping layer, passivating layer, hydrophobic layer, absorbers, and high PCE. This chapter explores recent developments and accomplishments involved in combining 3D and 2D perovskites for improving both the device efficiency along with ambient stability. This approach will provide the way ahead for research in the field of mixed 3D and 2D perovskite-based solar cells and their commercialization.

Acknowledgements The author, ADS, would like to thank the Science and Engineering Research Board (SERB), Department of Science and Technology (DST), New Delhi, India, for the financial support under, INSPIRE Faculty Award Number DST/INSPIRE/04/2015/002601 and SERB-Research Scientist award number SB/SRS/2021-2022/62/PS.

Author Contributions “The manuscript was written through the contributions of all the authors. All authors have given approval to the final version of the manuscript.”

References

- Akkerman, Q.A., Rainò, G., Kovalenko, M.V., Manna, L.: *Nat. Mater.* **17**, 394–405 (2018)
- Akkerman, Q.A., Manna, L.: *ACS Energy Lett.* **5**, 604–610 (2020)
- Bhosale, M.K., Kazi, A.I., Pawar, K.K., Shingate, R.S., Kadam, A.D., Patil, N.J., Sheikh, A.D.: *Nanotechnology* **34**, 065501 (2023)
- Bouduban, M.E.F., et al.: *J. Phys. Chem. Lett.* **10**, 5713–5720 (2019)
- Cao, D.H., Stoumpos, C.C., Yokoyama, T., Logsdon, J.L., Song, T.B., Farha, O.K., Wasielewski, M.R., Hupp, J.T., Kanatzidis, M.G.: *ACS Energy Lett.* **2**, 982–990 (2017)
- Chen, J., Lee, D., Park, N.G.: *ACS Appl. Mater. Interfaces.* **9**, 36338–36349 (2017)
- Cheng, P., et al.: *ACS Energy Lett.* **3**, 1975–1982 (2018)
- Cho, K.T., et al.: *Eng. Env. Sci.* **11**, 952–959 (2018)
- Cho, K.T. et al.: *Nano Lett.* **18**, 5467–74 (2018)
- Choi, W.G., Park, C.G., Kim, Y., Moon, T.: *ACS Energy Lett.* **5**, 3461–3467 (2020)

- Conings, B., et al.: *Adv. Mater.* **26**, 2041–2046 (2014)
- Deshpande, S.V., Bhiungade, R.A., Deshpande, M.P., Pawar, K.K., Bhat, T.S., Kulkarni, S.K., Sheikh, A.D.: *Mater. Res. Bull.* **142**, 111433 (2021)
- Efat, J., Po, Y.C., Chia, Y.L., Narra, S., Shahbazi, S., Diau, E.W.G.: *ACS Energy Lett.* **6**, 485–492 (2021)
- Gangadharan, D.T., Ma, D.: *Energy Environ. Sci.* **12**, 2860–2889 (2019)
- Gao, L., Zhang, F., Xiao, C., Chen, X., Larson, B.W., Berry, J.J., Zhu, K.: *Adv. Fun. Mater.* **29**, 1901652 (2019)
- Garai, R., Gupta, R.K., Hossain, M., Iyer, P.K.: *J. Mater. Chem. A* **9**, 26069 (2021)
- Ge, C., Xue, Y.Z.B., Li, L., Tang, B., Hu, H.: *Front. Mater.* **7**, 601179 (2020)
- Grancini, G. et al.: *Nat. Commun.* **8**, 15684 (2017)
- Grancini, G., Nazeeruddin, M.K.: *Nat. Rev. Mater.* **4**, 4–22 (2019)
- Grätzel, M.: *Nature* **414**, 338 (2001)
- Green, M.A., Dunlop, E.D., Ebinger, J.H., Yoshita, M., Kopidakis, N., Hao, X.: *Prog. Photovoltaics* **28**, 629 (2020)
- <https://www.nrel.gov/cell-efficiency>
- Hammarström, L., Hammes-Schiffer, S.: *Acc. Chem. Res.* **42**, 1859 (2009)
- Haque, M.A., Sheikh, A.D., Guan, X., Wu, T.: *Adv. Energy Mater.* **7**, 1602803 (2017)
- Jeon, N.J., Noh, J.H., Kim, Y.C., Yang, W.S., Ryu, S., Seok, S.I.: *Nat. Mater.* **13**, 897 (2014a)
- Jeon, N.J., et al.: *Nature Mater.* **13**, 897–903 (2014b)
- Jeon, N., Noh, J., Yang, W., et al.: *Nature* **517**, 476–480 (2015)
- Jung, E.H., Jeon, N.J., Park, E.Y., Moon, C.S., Shin, T.J., Yang, T.Y., Noh, J.H., Seo, J.: *Nature* **567**, 511–515 (2019a)
- Jung, E.H., et al.: *Nature* **567**, 511–515 (2019b)
- Kim, E.B., Akhtar, M.S., Shin, H.S., Ameen, S., Nazeeruddin, M.K.J.: *Photochem. Photobiol. c: Photochem. Rev.* **48**, 100405 (2021)
- Kim, J.S., Heo, J.M., Park, G.S., Woo, S.J., Cho, C., Yun, H.J., Kim, D.H., Park, J., Lee, S.C., Park, S.H., Yoon, E., Greenham, N.C., Lee, T.W.: *Nature* **611**, 688–694 (2022)
- Koh, T.M., Shanmugam, V., Schlipf, J., Oesinghaus, L., Buschbaum, P.M., Ramakrishnan, N., Swamy, V., Mathews, N., Boix, P.P., Mhaisalkar, S.G.: *Adv. Mater.* **28**, 3653 (2016)
- Koh, T.M., Shanmugam, V., Guo, X., Lim, S.S., Filonik, O., Herzig, E.M., Buschbaum, P.M., Swamy, V., Chien, S.T., Mhaisalkar, S.G., Mathews, N.: *J. Mater. Chem. A* **6**, 2122–2128 (2018)
- Kojima, A., Teshima, K., Shirai, Y., Miyasaka, T.: *J. Am. Chem. Soc.* **131**, 6050 (2009)
- Krishna, A., Gottis, S., Nazeeruddin, M.K., Sauvage, F.: *Adv. Funct. Mater.* **29**, 1806482 (2019)
- Lai, H., et al.: *J. Am. Chem. Soc.* **140**, 11639–11646 (2018)
- Lee, D.G., Kim, M., Wang, S., Kim, B.J., Meng, Y.S., Jung, H.S.: *ACS Appl. Mater. Interfaces* **51**, 48497–48504 (2019)
- Li, X., Bi, D., Yi, C., Décoppet, J.D., Luo, J., Zakeeruddin, S.M., Hagfeldt, A., Grätzel, M.: *Science* **353**, 58 (2016)
- Li, M.H., Yeh, H.H., Chiang, Y.H., Jeng, U.S., Su, C.J., Shiu, H.W.: *Adv. Mater.* **30**, 1801401 (2018)
- Liang, P.W., et al.: *Adv. Mater.* **26**, 3748–3754 (2014)
- Liang, C., Gu, H., Xia, Y., et al.: *Nat. Energy* **6**, 38–45 (2021)
- Liu, B., Long, M., Cai, M., Ding, L., Yang, J.: *Nano Energy* **59**, 715–720 (2019a)
- Liu, Y., Akin, S., Pan, L., Uchida, R., Arora, N., Milić, J.V., Hinderhofer, A., Schreiber, F., Uhl, A.R., Zakeeruddin, S.M., Hagfeldt, A., Dar, M.I., Grätzel, M.: *Sci. Adv.*, 5 eaaw2543 (2019)
- Ma, L., Ke, W., Pedesseau, L., Wu, Y., Katan, C., Even, J., Wasielewski, M.R., Stoumpos, C.C., Kanatzidis, M.G.: *J. Am. Chem. Soc.* **140**, 3775–3783 (2018)
- Ma, S., Yuan, G., Zhang, Y., Yang, N., Li, Y., Chen, Q.: *Energy Environ. Sci.* **15**, 13–55 (2022)
- Manjunath, V., Bimli, S., Shaikh, P.A., Ogale, S.B., Devan, R.S.: *J. Mater. Chem. C* **10**, 15725–15780 (2022)
- Mao, L., Ke, W., Pedesseau, L., Wu, Y., Katan, C., Even, J., Wasielewski, M.R., Stoumpos, C.C., Kanatzidis, M.G.: *J. Am. Chem. Soc.* **140**, 3775–3783 (2018)

- Mei, A., Li, X., Liu, L., Ku, Z., Liu, T., Rong, Y., Xu, M., Hu, M., Chen, J., Yang, Y., Grätzel, M., Han, H.: *Science* **345**, 295–298 (2014)
- Ortiz, C., Carmona, M.P., Solis, I.D.: *Chem. Sus. Chem.* **12**, 1560–1575 (2019)
- Quan, L., et al.: *J. Am. Chem. Soc.* **138**, 2649–2655 (2016)
- Quintero, B.R., et al.: *Nat. Mater.* **17**, 900–907 (2018)
- Saliba, M., Matsui, T., Domanski, K., Seo, J.Y., Ummadisingu, A., Zakeeruddin, S.M., Correa-Baena, J.P., Tress, W.R., Abate, A., Hagfeldt, A., Grätzel, M.: *Science* **354**, 206 (2016)
- Satapathi, S.: *ACS Energy Lett.* **7**, 906–907 (2022)
- Schileo, G., Grancini, G.: *J. Phys. Energy* **2**, 021005 (2020)
- Shamsi, J., Urban, A.S., Imran, M., Trizio, L.D., Manna, L.: *Chem. Rev.* **119**, 3296–3348 (2019)
- Sheikh, A.D., Bera, A., Haque, M.A., Rakhi, R.B., Gobbo, S.D., Alshareef, H.N., Wu, T.: *Sol. Eng. Mater. Sol. Cells* **137**, 6–14 (2015)
- Sheikh, A.D., Munir, R., Haque, M.A., Bera, A., Hu, W., Shaikh, P., Amassian, A., Wu, T.: *ACS App. Mater. Inter.* **9**, 35018–35029 (2017)
- Sheikh, A.D., Patil, A.P., Mali, S.S., et al.: *J. Mater. Sci.* **54**, 10825–10835 (2019)
- Sheikh, A.D., Vhanalakar, V.K., Katware, A.S., Pawar, K.K., Kulkarni, S.K.: *J. Alloys Compounds* **894**, 162388 (2022)
- Smith, I.C., Hoke, E.T., Ibarra, D.S., McGehee, M.D., Karunadasa, H.I.: *Angew. Chem.* **126**, 11414 (2014a)
- Smith, I.C., Hoke, E.T., Solis-Ibarra, D., McGehee, M.D., Karunadasa, H.I.: *Angewandte Chemie Int. Edi.* **53**, 11232–11235 (2014b)
- Soe, C.M.M., Stoumpos, C.C., Kepenekian, M., Traoré, B., Tsai, H., Nie, W., Wang, B., Katan, C., Seshadri, R., Mohite, A.D., Even, J., Marks, T.J., Kanatzidis, M.G.: *J. Am. Chem. Soc.* **139**, 16297–16309 (2017)
- Soe, C.M.M., Nie, W., Stoumpos, C.C., Tsai, H., Blancon, J.C., Liu, F., Even, J., Marks, T.J., Mohite, A.D., Kanatzidis, M.G.: *Adv. Eng. Mater.* **8**, 1700979 (2018)
- Stoumpos, C.C., Soe, C.M.M., Tsai, H., Nie, W., Blancon, J.C., Cao, D.H., Liu, F., Traoré, B., Katan, C., Even, J., Mohite, A.D., Kanatzidis, M.G.: *Chemistry* **2**, 427 (2017)
- Tsai, H., Nie, W., Blancon, J.C., Stoumpos, C.C., Asadpour, R., Harutyunyan, B., Neukirch, A.J., Verduzco, R., Crochet, J.J., Tretiak, S., Pedesseau, L., Even, J., Alam, M.A., Gupta, G., Lou, J., Ajayan, P.M., Bedzyk, M.J., Kanatzidis, M.G., Mohite, A.D.: *Nature* **536**, 312 (2016)
- Tsai, H., et al.: *Nat. Commun.* **9**, 2130 (2018)
- Ugur, E., Sheikh, A.D., Munir, R., Khan, J.I., Barrit, D., Amassian, A., Laquai, F.: *ACS Energy Lett.* **2**, 1960–1968 (2017)
- Wang, Z., Lin, Q., Chmiel, F.P., Sakai, N., Herz, L.M., Snaith, H.J.: *Nature Eng.* **2**, 17135 (2017)
- Wu, G., Li, X., Zhou, J., Zhang, J., Zhang, X., Leng, X., Wang, P., Chen, M., Zhang, D., Zhao, K., Liu, S., Zhou, H., Zhang, Y.: *Adv. Mater.* **31**, 1903889 (2019a)
- Wu, G., et al.: *Adv. Mater.* **31**, 1903889 (2019b)
- Xiao, Z.G., et al.: *Energy Environ. Sci.* **7**, 2619–2623 (2014)
- Yang, W.S., et al.: *Science* **348**, 1234–1237 (2015)
- Yao, K., Wang, X., Li, F., Zhou, L.: *Chem. Comm.* **51**, 15430–15433 (2015)
- Yao, K., Wang, X., Xu, Y.X., Li, F., Zhou, L.: *Chem. Mater.* **28**, 3131–3138 (2016)
- Yoo, J.J., Wieghold, S., Sponseller, M.C., Chua, M.R., Bertram, S.N., Hartono, N.T.P., Tresback, J.S., Hansen, E.C., Correa-Baena, J.P., Bulović, V., Buonassisi, T., Shin, S.S.: *Bawendi MG. Energy Environ. Sci.* **12**, 2192–2199 (2019)
- You, J., et al.: *Appl. Phys. Lett.* **105**, 183902 (2014)
- Younis, A., Lin, C.H., Guan, X., Shahrokhi, S., Huang, C.Y., Wang, Y., He, T., Singh, S., Hu, L., Retamal, J.R.D., He, J.H., Wu, T.: *Adv. Mater.* 2005000 (2021)
- Yukta, P.N., Chavan, R.D., Yadav, P., Nazeeruddin, M.K., Satapathi, S.: *ACS Appl. Mater. Interfaces* **14**(26), 29744–29753 (2022)
- Zhang, J., Hu, B.: *Nano Energy* **76**, 104999 (2020)
- Zhang, X., Wu, G., Yang, S., Fu, W., Zhang, Z., Chen, C., Liu, W., Yan, J., Yang, W., Chen, H.: *Small* **13**, 1700611 (2017a)

- Zhang, T., Dar, M.I., Li, G., Xu, F., Guo, N., Grätzel, M., Zhao, Y.: *Sci. Adv.* **3**, e1700841 (2017b)
- Zhang, F., Kim, D., Zhu, K.: *Curr. Opin. Electrochem.* **11**, 105–113 (2018)
- Zhang, J., Qin, J., Wang, M., Bai, Y., Zou, H., Keum, J.K., Tao, R., Xu, H., Yu, H., Haacke, S., Hu, B.: *Joule* **3**, 3061–3071 (2019b)
- Zhang, F., Lu, H., Tong, J., Berry, J.J., Beard, M., Zhu, K.: *Energy Environ. Sci.* **13**, 1154–1186 (2020)
- Zhang, J., Qin, J., Wang, M., Bai, Y., Zou, H., Keum, J.K., Tao, R., Xu, H., Yu, Haacke, S., Hu, B.: *Joule* **3**, 3061–3071 (2019)
- Zhou, N., et al.: *J. Am. Chem. Soc.* **140**, 459–465 (2017)
- Zuo, C., Scully, A.D., Vak, D., Tan, W., Jiao, X., McNeill, C.R., Angmo, D., Ding, L., Gao, M.: *Adv. Eng. Mater.* **9**, 1803258 (2019)